

High Stability of a Donor–Acceptor Type Oxazepine-Containing Fluorophore and Its Applications in Cellular Imaging and Two-Photon Deep Tissue Imaging

Heejo Moon,^{†,◆} Yuna Jung,^{§,◆} Youngseo Kim,^{¶,◆} Byeong Wook Kim,[†] Jin Gyu Choi,[▽] Na Hee Kim,[§] Myung Sook Oh,^{▽,||} Sungnam Park,^{*,||,Ⓜ} B. Moon Kim,^{*,†,Ⓜ} and Dokyoung Kim^{*,§,△,±,#,Ⓜ}

[†]Department of Chemistry, College of Natural Sciences, Seoul National University, Seoul 08826, Republic of Korea

[§]Department of Biomedical Science, Graduate School, [▽]Department of Life and Nanopharmaceutical Science, Graduate School,

^{||}Department of Oriental Pharmaceutical Science, College of Pharmacy and Kyung Hee East-West Pharmaceutical Research Institute, [△]Department of Anatomy and Neurobiology, College of Medicine, [±]Center for Converging Humanities, [#]Medical Research Center for Bioreaction to Reactive Oxygen Species and Biomedical Science Institute, Kyung Hee University, Seoul 02247, Republic of Korea

[¶]Department of Chemistry, Korea University, Seoul 02841, Republic of Korea

Supporting Information

ABSTRACT: A new donor (D)–acceptor (A) type naphthalene-based oxazepine-containing fluorophore, OXN-1, is reported, which shows unusually high stability in various environments. Its photophysical properties and structural stabilities under harsh conditions are thoroughly examined. The high stability of OXN-1 is explained by quantum chemical calculations. Its exceptional bioimaging capabilities for cells with low cytotoxicity are verified. In addition, its deep tissue imaging ability with two-photon microscopy (TPM) is evaluated.



Oxazepines are unsaturated heterocycles of seven atoms containing oxygen and nitrogen.¹ Some oxazepines show interesting biological and pharmaceutical characteristics, such as antitumor,² anti-inflammation,³ and antimicrobial activities.⁴ Medically important drugs, such as Amoxapine,⁵ Loxapine,⁶ and Nitroxazepine,⁷ have oxazepine backbone with hybridization of two benzene rings (Figure 1a).

Recently, our research group has focused on the development of naphthalene-based platforms for new fluorophores and pharmacophores by introducing several functional groups, such as amine, aldehyde, and hydroxy moiety on the naphthalene core.^{8,9} More recently, we successfully synthesized a D–A type oxazepine-containing naphthalene-based fluorophore, OXN-1, and have found that OXN-1 exhibits an unusually high stability in various severe environments, such as acidic or basic pH levels (pH 4–9), biological fluids, intensive light exposure, and hydrolysis (Figure 1b). For various biological applications, the high stability of fluorophores under harsh conditions and their low cytotoxicity are essential. In this sense, OXN-1 is found to be an excellent fluorophore and be of potential use for bioimaging as shown below.

Generally, most medically applicable oxazepine derivatives have aniline type heterocycles, which are moderately stable for the hydrolysis of C=N or OC–N bond in aqueous media.¹⁰ In this study, the synthesized OXN-1 has an imine bond in the [1,4] oxazepine backbone with monohybridization of naphthalene, and this is the first example of naphthalene-oxazepine platforms (Figure 1b). The imine bond in the oxazepine works as an electron acceptor (A) and the dimethylamine group works

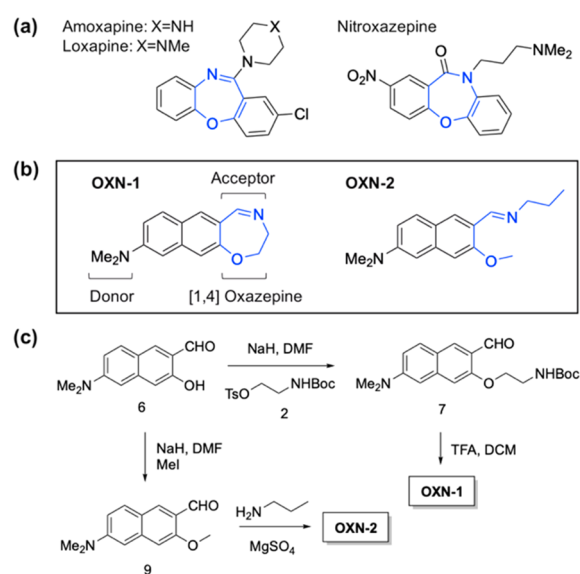


Figure 1. (a) Molecular structures of representative oxazepines (blue) containing pharmacophore; Amoxapine, Loxapine, and Nitroxazepine. (b) Molecular structure of OXN series; OXN-1 and OXN-2. (c) Synthesis of OXN-1 and OXN-2.

Received: March 3, 2019

as an electron donor (D) that shows intramolecular charge transfer (ICT) characteristics on the naphthalene bridge,¹¹ which is a typical structural feature of fluorescent molecules.

OXN-1 was prepared from the 6-(dimethylamino)-3-hydroxy-2-naphthaldehyde (6),⁸ through two-step reactions, i.e., (i) *O*-alkylation with 2-((*tert*-butoxycarbonyl)amino)ethyl 4-methylbenzenesulfonate and (ii) *N*-Boc deprotection with trifluoroacetic acid (TFA) (Figure 1c). OXN-1 was isolated in the *N*-Boc deprotection step of aminoethoxy moiety on the naphthaldehyde backbone of 7 presumably through subsequent fast intramolecular ring-formation (Scheme S1). The imine formation was verified by NMR analysis (¹H, ¹³C) as well as high-resolution mass spectrometry, and it is found to be thermodynamically favorable (99% yield). It is well-known that some moieties like imine, amide, and nitrile on the acceptor site (2-position) of naphthalene backbone are responsible for blue fluorescence in the range from 400 to 500 nm.^{9,12} Interestingly, however, we observed bright yellowish fluorescence from isolated OXN-1 in aqueous media under 365 nm irradiation, so we systematically investigated the photophysical property of OXN-1 in various environments. To understand the effects of oxazepine (cyclic-imine) moiety, we prepared a noncyclic imine, OXN-2 (Figure 1b), as a control compound, and compared its photophysical properties with those of OXN-1 (Figure 2).

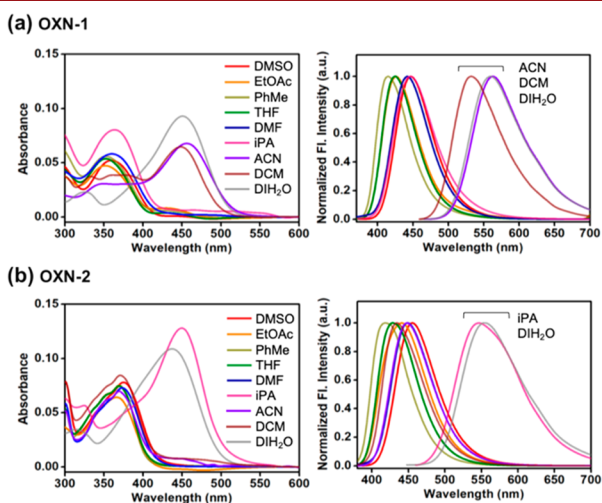


Figure 2. (a,b) UV/vis absorption (left) and fluorescence spectra (right) of OXN series in various solvents. All measurements were performed at 25 °C in the given solvent. The spectra were recorded after excitation at the maximum UV/vis absorption wavelength (Table S1).

First, we studied the UV/vis absorption and fluorescence spectra of OXN series in various solvents, as presented in Figure 2 and Table S1 (see also Figures S1 and S2). The absorption and emission peaks of OXN series in organic solvents are observed in the UV and visible wavelengths ($\lambda_{\text{abs}} = 320\text{--}400$ nm, $\lambda_{\text{emi}} = 400\text{--}500$ nm), but they are red-shifted significantly to the longer wavelengths ($\lambda_{\text{abs}} = 400\text{--}500$ nm, $\lambda_{\text{emi}} = 500\text{--}700$ nm) in aqueous media (Figure 2a,b, Table S1). Interestingly, such a large bathochromic shift of OXN-1 was also observed in acetonitrile (ACN) and dichloromethane (DCM), which are polar aprotic solvents, while OXN-2 shows a large bathochromic shift only in a polar protic solvent (i.e., isopropyl alcohol; iPA). In addition, a large Stokes shift is observed in OXN-1 ($\Delta\lambda = 108$ nm) and OXN-2 ($\Delta\lambda = 118$ nm) in deionized water (DI H₂O).

The large Stokes shift results from the ICT in OXN series and the solvent polarity, and it is a typical feature of D–A type fluorophores.¹¹ The fluorescence intensities of OXN series are relatively strong in dimethyl sulfoxide (DMSO) exhibiting the quantum yields of OXN-1 (QY = 0.70) and OXN-2 (QY = 0.61), whereas it shows a minimal effect in DI H₂O (Figures S2 and S3). This is also a typical property of D–A type fluorophores due to the hydrogen-bond induced decrement of ICT and nonradiative decays in the excited state.¹¹ Time-resolved fluorescence (TRF) experiments were used to determine the fluorescence lifetimes of OXN-1 ($\tau = 4.4$ ns) and OXN-2 ($\tau = 4.0$ ns), which is in the typical lifetime of organic fluorophores (Figure S4).

After studying the basic photophysical properties, we examined the chemical stability of OXN series in various environments using liquid chromatography–mass spectrometry (LC–MS) and fluorescence spectroscopy (Figure 3). As the

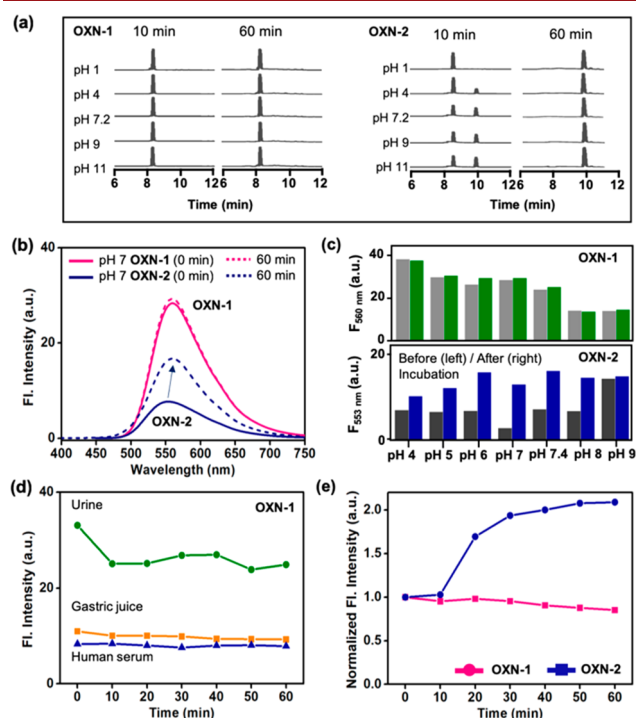


Figure 3. (a) Hydrolytic stability test results of OXN-1 (left) and OXN-2 (right) using LC–MS. (b) Fluorescence spectra of OXN-1 (5 μ M, pink solid line) and OXN-2 (5 μ M, blue solid line) measured after 60 min incubation (dot lines) at 25 °C in pH 7 buffer. (c) Plot of fluorescence intensities of OXN series (5 μ M) as a function of pH level. The fluorescence intensities are measured at the maximum fluorescence wavelength (at 560 nm for OXN-1 and at 553 nm for OXN-2) before and after 60 min incubation at 25 °C. (d) Plot of fluorescence intensities of OXN-1 (5 μ M) in various biofluids (mouse urine, mouse gastric juice, and human serum) as a function of incubation time at 25 °C. (e) Plot of normalized fluorescence intensities of OXN-1 (5 μ M) and OXN-2 (5 μ M) as a function of irradiation time under continuous 365 nm LED light irradiation (approximately 6 W at a focal plane) in DI H₂O.

imine bond has low stability under hydrolytic conditions, the imine containing fluorophore is not commonly used for the bioimaging. In the first test, we exposed the OXN series to various pH levels from acidic (pH 1) to basic (pH 11) including physiological pH 7.2. Surprisingly, no hydrolysis product of OXN-1 was observed in LC–MS analysis (OXN-1 peak at 8.27

min) for the sufficiently long incubation time (10–60 min, 1–24 h) at each pH at 25 °C (Figures 3a and S5). In contrast, OXN-2 containing a noncyclic imine showed a new peak at 9.9 min at most pH levels after 10 min incubation. This new peak resulted from an imine hydrolyzed product; naphthaldehyde (Figure S6), which was further confirmed by ESI Q-TOF mass spectrum ($m/z = 229.10$), and the hydrolysis was found to be completed within a 60 min incubation period.

Next, we examined the fluorescence spectra of OXN series after incubation at various pH levels. At pH 7.0, the fluorescence intensity of OXN-1 was observed to be higher than that of OXN-2 before incubation (3.7 times, Figure 3b). After 60 min incubation at pH 7, OXN-1 showed no significant change in the fluorescence spectrum in terms of its peak position and intensity as expected (Figures 3b,c and S7). In contrast, OXN-2 showed a large increase in fluorescence intensity (2.2 times increase) and a slight blue shift of its peak position (553 to 559 nm) due to the generation of hydrolysis products, 6-(dimethylamino)-3-(methoxy)-2-naphth-aldehyde (6-DMMNA) (Figure S6, compound 9 in Scheme S1), and the similar results were observed at all pH levels we tested (Figure 3c). For further verification, we compared the UV/vis absorption and fluorescence spectra for both OXN-2 and 6-DMMNA (Figure S6). The high stability of OXN-1 was also confirmed in the biofluids at different pH levels; mouse urine (pH 5.0), mouse gastric juice (pH 3.0, fed), and human serum (pH 7.4) (Figures 3d and S8). This biofluid assay result represents that OXN-1 can be employed to study complex biological samples under extreme environmental conditions.

We also evaluated the photostability of OXN-1 in aqueous media (Figure 3e). OXN-1 was observed under strong UV irradiation (365 nm, 6 W), for up to 60 min incubation time, and a negligible fluorescence intensity change was observed. OXN-2, however, showed a gradual increment of fluorescence intensity, as its imine was hydrolyzed and produced 6-DMMNA (Figure S9).

The optimized molecular structures, HOMO–LUMO energy levels, and absorption spectra were obtained by quantum chemical calculations (Figures S10 and 4a,b). In addition, the Mulliken atomic charges of OXN series and their protonated forms were calculated (Figure 4a,b). In the acidic hydrolysis of imine, protonation of the imine nitrogen occurs as a first step, and then a water molecule is added to the imine carbon as a second step (Figure S11). The Mulliken atomic charges provide important mechanistic clues for the stability of OXN-1 in the hydrolysis. Based on the atomic charges of the imine nitrogen (-0.253 au for OXN-1 and -0.179 au for OXN-2), the imine nitrogen in OXN-1 is expected to be slightly more protonated than that in OXN-2 (Figure 4a). However, in the second step, the nucleophilic addition of a water molecule to the imine carbon is much less likely in OXN-1 than OXN-2 due to a large negative charge on the imine carbon (-0.474 au for OXN-1 vs -0.011 au for OXN-2) (Figure 4b). In addition, the large negative atomic charge on the imine carbon in OXN-1 is repulsive for direct nucleophilic addition of a water molecule in the hydrolysis (Figure 4a). For these reasons, OXN-1 is found to be highly stable in the hydrolysis.

In order to explore the potential of OXN-1 for bioimaging applications further, we applied OXN-1 to cells and collected the fluorescence imaging using confocal laser scanning microscopy (CLSM). Prior to the imaging study, a high cell viability; >95% with 0–100 μM concentration of OXN-1 in HeLa cell (immortalized human cervical cancer cell) was measured by MTT assay (Figure 5a). Also, the high stability of OXN-1 at high

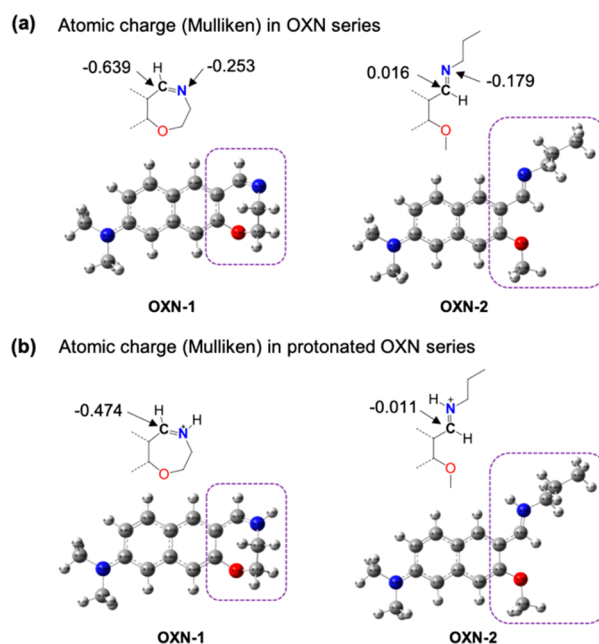


Figure 4. (a,b) Comparison of atomic charges in acceptor units of OXN series and their protonated forms. The numbers are the Mulliken atomic charges.

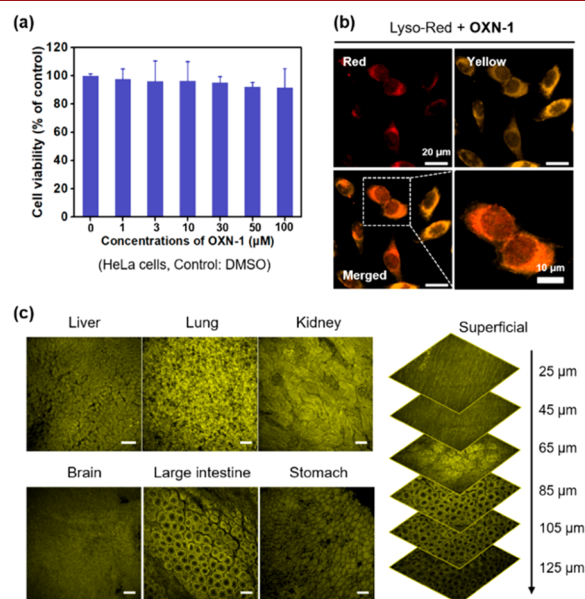


Figure 5. (a) Cell viability of OXN-1. HeLa cells were incubated with OXN-1 (0–100 μM) for 24 h. The means and standard deviations were calculated from triplicate measurements. (b) CLSM images of HeLa cells coincubated with OXN-1 (20 μM) with lysozyme imaging agent (LysoTracker Deep-Red; Lyso-Red, 5 $\mu\text{g}/\text{mL}$) for 30 min incubation at 37 °C. Excitation wavelength and emission channel; OXN-1 (450 nm, 450–617 nm), Lyso-Red (645 nm, 645–700 nm). (c) TPM images of different mouse organ tissues incubated with OXN-1 at a middle depth layer (~ 85 μm) of sectioned tissues (left) and images of large intestine at the indicated depths (right). Scale bar: 100 μm (left), 200 μm (right). See the experimental details in the Supporting Information.

concentration of biothiol, glutathione (GSH, 10 mM), was confirmed (Figure S12). To investigate the cell organelle specificity of OXN-1, we conducted a costaining experiment with commercialized reagents, MitoTracker Deep-Red (target to mitochondria) and LysoTracker Deep-Red (target to

lysosome), respectively (Figures 5b and S13). The merged image indicated that the OXN-1 is mainly localized in the lysosome that has slightly acidic pH, presumably due to the amine moieties in the structure.

Next, we demonstrated the two-photon tissue imaging ability of OXN-1. With the sizable two-photon action cross-section (TPACS, GM; Goepfert-Mayer unit) value of OXN-1 (14 GM at 840 nm, 15 GM at 860 nm) (Figure S14), we observed bright TPM tissue images from several mouse organs (liver, lung, kidney, brain, large intestine, stomach) (Figures 5c, S15, and S16). The depth-dependent TPM imaging result represented the high tissue permeability and deep tissue imaging ability of OXN-1.

Under the given imaging condition for CLSM and TPM, autofluorescence interference from the intrinsic biomolecules such as riboflavin, NADH, etc., was negligible (Figures S13 and S15).

In conclusion, we synthesized a new D–A type oxazepine-containing naphthalene-based fluorophore, OXN-1, and discovered that it exhibits unusually high stability with superior photophysical properties. OXN-1 holds promise as a new class of dyes in the development of fluorescent probes because it maintains strong fluorescence in biofluids as well as under UV irradiation and has a high biocompatibility with lysosome-selective staining properties. In addition, we expect that OXN-1 can be used as a stable dye in biomedical field since it shows superior two-photon deep-tissue imaging ability from the various organ tissues.

■ ASSOCIATED CONTENT

● Supporting Information

The Supporting Information is available free of charge on the ACS Publications website at DOI: 10.1021/acs.orglett.9b00784.

Experimental details, spectroscopic data, bioimaging data, and characterization; ¹H and ¹³C NMR spectra (PDF)

■ AUTHOR INFORMATION

Corresponding Authors

*E-mail: dkim@khu.ac.kr.

*E-mail: kimbm@snu.ac.kr.

*E-mail: spark8@korea.ac.kr.

ORCID

Sungnam Park: 0000-0001-6288-4620

B. Moon Kim: 0000-0001-6924-268X

Dokyoung Kim: 0000-0002-7756-3560

Author Contributions

◆ These authors contributed equally.

Notes

The authors declare no competing financial interest.

■ ACKNOWLEDGMENTS

This research was supported by the Bio & Medical Technology Development Program of the NRF of Korea funded by the Ministry of Science & ICT (2018-M3A9H3021707). This research was also supported by Basic Science Research Program through the NRF of Korea funded by the ministry of Education (2018-R1A6A1A03025124, 2018-R1D1A1B07043383). B.M.K. thanks the financial support from the NRF of Korea (2012-M3A7B4049644). S.P. thanks the financial support from the NRF of Korea (2016-R1A2B4011522).

■ REFERENCES

- (1) (a) Sangshetti, J. N.; Ansari Altamash Shakeel, A.; Kalam Khan, F. A.; Zaheer, Z. *Mini-Rev. Org. Chem.* **2015**, *12*, 345–354. (b) Shen, J.; Xue, L.; Lin, X.; Cheng, G.; Cui, X. *Chem. Commun.* **2016**, *52*, 3292–3295.
- (2) (a) Pan, W.; Liu, H.; Xu, Y.-J.; Chen, X.; Kim, K. H.; Milligan, D. L.; Columbus, J.; Hadari, Y. R.; Kussie, P.; Wong, W. C.; Labelle, M. *Bioorg. Med. Chem. Lett.* **2005**, *15*, 5474–5477. (b) Singh, A. K.; Bhadauria, A. S.; Kumar, U.; Raj, V.; Rai, A.; Kumar, P.; Keshari, A. K.; Kumar, D.; Maity, B.; Nath, S.; Prakash, A.; Saha, S. *Sci. Rep.* **2018**, *8*, 5932. (c) Binaschi, M.; Boldetti, A.; Gianni, M.; Maggi, C. A.; Gensini, M.; Bigioni, M.; Parlani, M.; Giolitti, A.; Fratelli, M.; Valli, C.; Terao, M.; Garattini, E. *ACS Med. Chem. Lett.* **2010**, *1*, 411–415.
- (3) Chakrabarti, J. K.; Hicks, T. A. *Eur. J. Med. Chem.* **1987**, *22*, 161–163.
- (4) (a) Basavaraju, B.; Bhojya Naik, H. S.; Prabhakara, M. C. *Bioinorg. Chem. Appl.* **2007**, *2007*, 42587. (b) Bonsignore, L.; De Logu, A.; Loy, G.; Lavagna, S. M.; Secci, D. *Eur. J. Med. Chem.* **1994**, *29*, 479–485.
- (5) Jue, S. G.; Dawson, G. W.; Brogden, R. N. *Drugs* **1982**, *24*, 1–23.
- (6) Popovic, D.; Nuss, P.; Vieta, E. *Ann. Gen. Psychiatry* **2015**, *14*, 15–15.
- (7) Blackwell, B. In *Side Effects of Drugs Annual*; Dukes, M. N. G., Ed.; Elsevier, 1977; Vol. 1.
- (8) (a) Kim, D.; Moon, H.; Baik, S. H.; Singha, S.; Jun, Y. W.; Wang, T.; Kim, K. H.; Park, B. S.; Jung, J.; Mook-Jung, I.; Ahn, K. H. *J. Am. Chem. Soc.* **2015**, *137*, 6781–6789. (b) Kim, D.; Baik, S. H.; Kang, S.; Cho, S. W.; Bae, J.; Cha, M.-Y.; Sailor, M. J.; Mook-Jung, I.; Ahn, K. H. *ACS Cent. Sci.* **2016**, *2*, 967–975.
- (9) Jung, Y.; Kim, Y.; Kim, N. H.; Lee, J.; Kim, K.-H.; Jung, J.; Huh, Y.; Jang, H.-J.; Joo, J.; Park, S.; Kim, D. *Dyes Pigm.* **2019**, *162*, 104–111.
- (10) Goutham, K.; Ashok Kumar, D.; Suresh, S.; Sridhar, B.; Narender, R.; Karunakar, G. V. *J. Org. Chem.* **2015**, *80*, 11162–11168.
- (11) Singha, S.; Kim, D.; Roy, B.; Sambasivan, S.; Moon, H.; Rao, A. S.; Kim, J. Y.; Joo, T.; Park, J. W.; Rhee, Y. M.; Wang, T.; Kim, K. H.; Shin, Y. H.; Jung, J.; Ahn, K. H. *Chem. Sci.* **2015**, *6*, 4335–4342.
- (12) (a) Wang, J.-Y.; Liu, Z.-R.; Ren, M.; Lin, W. *Sci. Rep.* **2017**, *7*, 1530. (b) Tang, Y.; Jiang, G.-F. *New J. Chem.* **2017**, *41*, 6769–6774.